In-vivo targeted tagging of RNA isolates cell specific transcriptional responses to environmental stimuli and identifies liver-to-adipose RNA transfer

Darr J. [1,2], Lassi M.[1,2], Archana Tomar[1,2], Gerlini R.[1,2], Scheid F.[1,2], Hrabě de Angelis M.[1,2,3] Witting M.[4,5,#] and Teperino R.[1,2,#]

1 - Institute of Experimental Genetics, Helmholtz Zentrum München, German Research center for Environmental Health – Neuherberg, Germany
2 - German Center for Diabetes Research (DZD) – Neuherberg, Germany
3 - Experimental Genetics, Faculty of Life and Food Sciences Weihenstephan, Technische Universität München, Freising-Weihenstephan, Germany.
4 - Research Unit Analytical BioGeoChemistry, Helmholtz Zentrum München
5 - Chair of Analytical Food Chemistry, Technische Universität München, Freising, Germany

[#] To whom correspondence should be addressed:
(raffaele.teperino@helmholtz-muenchen.de , Michael.witting@helmholtz-muenchen.de)

Abstract

Bio-fluids contain various circulating cell-free RNA transcripts (ccfRNAs). The composition of these ccfRNAs varies between bio-fluids and constitute tantalizing biomarker candidates for several pathologies. ccfRNAs have also been demonstrated as mediators of cellular communication, yet little is known about their function in physiological and developmental settings and most works are limited to in-vitro studies. Here, we have developed iTAG-RNA, a novel method for the unbiased tagging of RNA transcripts in mice in-vivo. We used this method to isolate hepatocytes and kidney proximal epithelial cells-specific transcriptional response to a dietary challenge without interfering with the tissue architecture, and to identify multiple hepatocyte-secreted ccfRNAs in plasma. We also identified transfer of these hepatic derived ccfRNAs to adipose tissue, where they likely serve as a buffering mechanism to maintain cholesterol and lipid homeostasis. Our findings directly demonstrate in-vivo transfer of RNAs between tissues and highlight its implications for endocrine signaling and homeostasis.

Introduction

Little is known about the biological function of circulating cell-free RNAs (**ccfRNA**). Found to be associated with exosomes, lipoproteins, ribonucleoproteins and more, these transcripts can be isolated and sequenced from multiple bio-fluids such as plasma, lymph, cerebral fluids, breast milk and more [1, 2]. ccfRNAs are directly implicated in the development of several pathologies including cancer and obesity [3-5] and are intensively studied as disease biomarkers [6, 7]. Despite this, the role they play in physiological and developmental settings and in mediating cell-to-cell communication remains largely unknown. In-vitro, a growing number of works demonstrate the relevance of RNA based cellular communication [8-11], however in-vivo evidence is still limited. This discrepancy is partly due to the difficulties posed to tracking ccfRNAs from transcriptional source to potential sites of action in-vivo. Indeed the tools available to study ccfRNAs in physiological settings are limited and very few studies attempt to tackle this problem directly.

One work found evidence to suggest that the majority of circulating miRNAs originate in adipose tissue and that some of the adipose derived miRNAs may play a role in the regulation of liver Fgf21 levels [12]. However, this work focuses on miRNA and does not directly demonstrate transfer of RNAs between tissues nor directly identify adipose secreted RNAs.

Transfer of miRNAs was also demonstrated between epithelial cells of the caput epididymis to maturing spermatozoa, leading to a shift in sperm RNA content during its maturation [13]. This study made use of 4-thiouracil-tagging (TU-tagging) [14] combined with SLAM-Seq [15] to demonstrate loading of miRNAs transcribed in caput epididymis into maturing spermatozoa. TU-tagging entails cell-type specific expression of uracil phosphoribosyltransferase (UPRT) and administration of 4-thiouracil, with the assumption that only cells expressing UPRT would incorporate 4-thiouracil into transcribing RNA. Thio-RNA can then be purified and used for downstream gene expression analyses, or alternatively combined with SLAM-Seq to identify labeled transcripts. TU-tagging has proven useful in several additional systems [14, 16, 17], however, given endogenous [18] and alternative [19] pathways for uracil incorporation, the labeling specificity in this method remains unclear. In addition, as is demonstrated in Herzog et. al [15] and by Sharma et. al [13], labeling with TU-tagging of PolI and PolIII transcripts is inefficient, rendering tRNAs and ribosomal transcripts unlabeled.

Indeed there are only a limited number of techniques enabling in-vivo targeted labeling of RNAs. In addition to TU-tagging, 5-ethynylcytosine-tagging (EC-tagging) [20] is a new method, which utilizes cell-type specific co-expression of cytosine deaminase (CD) with UPRT to achieve RNA labeling with 5-ethynyluridine (5EU) following administration of 5-ethynylcytosine. Both TU and EC tagging use cre-recombination to express the relevant enzymes in a tissue specific manner and stochastic expression from the cre-promoter may lead to unwanted expression of the enzymes in different tissues [21]. Finally, one recently developed method called Mime-seq allows for cell type specific labeling of microRNA [22]. In this method, tissue specific expression of a plant derived methyltransferase mediates a 3′-terminal 2′-O-methylation of microRNAs that, when combined with a methylation dependent library construction, allows for sequencing of tissue specific microRNAs. Mime-seq allows labeling of miRNAs alone leaving other RNA biotypes unlabeled. Given the need for a technique that allows for a Cre-independent and unbiased labeling of total RNA transcription in-vivo, we developed iTAG-RNA **[For In-vivo Targeted Tagging of RNA]**. This method incorporates mouse genetics with a novel uridine analog and an established RNA labeling chemistry to allow tagging of total RNA in target cells in-vivo. Using iTAG-RNA we are able to identify transcriptional re-programming of hepatocytes in-vivo following an acute high fat diet stress and to enrich for and identify hepatocyte derived plasma ccfRNAs. Moreover, we are able to identify RNA-based liver-to-adipose RNA transfer. These liver derived ccfRNAs include variable coding and non-coding RNAs such as miRNAs and tRNAs. Among the miRNAs transferred from liver to adipose tissue we find mir-33, mir-10b and mir130a, which target major regulators of cholesterol and lipid efflux and bio-synthesis such as Srebf1 [23], Abca1 [23, 24], Ppara [25] and Pparg [26] respectively.

Our study demonstrates for the first time an unbiased technique that allows labelling, tracking and quantification of variable types of ccfRNAs from their transcriptional source to downstream tissues, in which they can potentially act to regulate expression of target genes. We demonstrate RNA-based liver-to-adipose transfer of a myriad of RNA transcripts and their response to an environmental challenge. The continued identification and characterization of RNA based signaling in-vivo is imperative for the understanding of developmental, physiological and pathological processes, and can aid in the future development of relevant disease biomarkers.

Results

93 **Small molecule design and genetic approach for targeted in-vivo labeling of RNA**
94 5-Ethynyl Uridine **(5EU)** is a synthetic uridine analogue extensively used in RNA turnover studies
95 [27-29]. The nitrogenous base contains an alkyne group that can be covalently linked to an azide
96 group using a simple copper mediated reaction called click chemistry [30, 31]. This synthetic base
97 has been demonstrated to incorporate into transcribing RNA in place of uridine and have little to
98 no biological effects thereafter [27]. Following administration to mice, 5EU is readily taken up by
99 cells with no regard to cell identity, depending to some extent on the administration method and
100 dosage used [27]. Here, we present a novel method for the targeted in-vivo delivery of 5EU.
101 To achieve this, we designed a 'pro-drug' of the 5EU base **(HD5EU)** that is based on the 'Hep-
102 Direct' pro-drug design [32, 33] **(Figure 1a)**. This design was developed to target small molecules
103 and nucleotide analogues to the human CYP3A4 enzyme and several small molecules of this
104 design have been or are currently in clinical studies [34-36]. The human CYP3A4 enzyme
105 catalyzes an oxidative cleavage of the HD5EU small molecule which, following a spontaneous
106 beta-elimination, results in the formation of 5EU mono-phosphate that can then be incorporated
107 into transcribing RNA **(Figure 1a)**. HD5EU was synthesized by Chiroblock GmbH, the identity
108 of the final product was validated using MS, p-NMR and h-NMR and the molecule's purity was
109 assessed at over 98% **(Sup. Figure 1a-d)**.
110 In addition to the HD5EU small molecule we took advantage of the published humanized liver
111 specific CYP3A4 mouse line **FVB/129P2-*Cyp3a13*^{tm1Ahs} Del(*5Cyp3a57-Cyp3a59*)^{1Ahs}**
112 **Tg(*APOE*-CYP3A4)^{A1Ahs}** obtained from Taconic [37, 38]. These humanized mice **(hCYP3A4)**
113 express the human CYP3A4 enzyme under a modified Apolipoprotein E (APOE) promoter and
114 are stably knocked out for nine homologous murine genes, thus leaving the human enzyme as the
115 sole member of the enzyme family to be expressed in a Cre-independent, tissue-specific manner
116 in-vivo. In keeping with published data on the activity of the modified ApoE promoter [39], qRT-
117 PCR and WB analyses demonstrate restricted expression of the human Cyp3a4 enzyme to liver
118 and kidney (**Figure 1b-c**). As such, upon administration of the HD5EU small molecule to the
119 humanized CYP3A4 mice, we expect the molecule to be metabolized to bioavailable 5EU mono-
120 phosphate exclusively in cells expressing CYP3A4, namely hepatocytes and kidney proximal renal
121 epithelial cells**,** thus allowing in-vivo targeted labelling of transcription and identification of
122 secreted transcripts in bio-fluids upon pull-down of 5EU labelled RNA (**Figure 1d**).
123

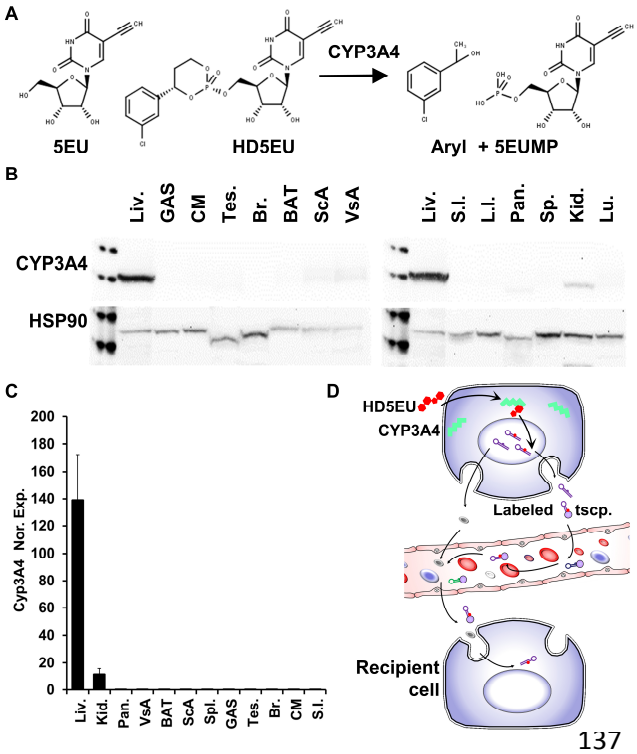

Figure 1. HD5EU small molecule design and CYP3A4 expression pattern. A) HD5EU small molecule and metabolite structure relative to 5EU. **B)** W.B. depicting tissue expression pattern of CYP3A4 in humanize CYP3A4 cluster deleted mice. HSP90 serves as loading control. GAS = Gastrocnemius muscle; CM = Cardiac Muscle; BAT = Brown adipose tissue; ScA = Subcutaneous white adipose tissue; VsA = Visceral white adipose tissue; S.I. = Small intestine; L.I. = Large intestine. **C)** qRT-PCR validating liver and kidney specific expression of CYP3A4. Error-bars for standard-deviation of 3 biological repeats. **D)** Administration of the HD5EU small molecule to cells expressing CYP3A4 allows metabolism to 5EU and labelling of total RNA. Labeled transcripts are then secreted to the extracellular matrix and can be identified in bio-fluids and recipient cells.

CYP3A4 is necessary for in-vitro and in-vivo metabolism of the HD5EU small molecule

To test and validate the metabolism of the HD5EU small molecule, we first isolated primary hepatocytes from hCYP3A4 mice. Following an 8 hour treatment of primary hepatocytes with 1mM HD5EU or 5EU, nuclear staining similar to 5EU labeling is clearly evident following click-it fluorescent staining **(Figure 2a)**. When pre-treated with Azamulin, a highly selective CYP3A4 inhibitor [40], HD5EU treated primary hepatocytes no longer demonstrate nuclear staining, in contrast to 5EU treated primary hepatocytes, where nuclear staining is unaffected by Azamulin pretreatment **(Figure 2a)**. These results indicate that while 5EU is still readily incorporated into transcribing RNA in the nucleus, nuclear staining in HD5EU treated cells is dependent upon CYP3A4 activity.

We administered HD5EU to humanized CYP3A4 mice and already 2 hours following administration found robust nuclear staining in hepatocytes and kidney epithelial cells but in no

155 other tissue examined. This in contrast to mice administered with 5EU where nuclear staining was
156 evident in multiple tissues **(Figure 2b-c and sup. Figure 2a).** Of note, animals administered with
157 HD5EU did not demonstrate any visible side effects. In addition we could not detect any signs of
158 DNA damage or apoptosis in the liver during the different treatment regimens as demonstrated by
159 staining for phosph-P53 and cleaved Caspase-3, supporting HD5EU as a non-toxic agent **(Sup**
160 **Figure 2b)**.
161

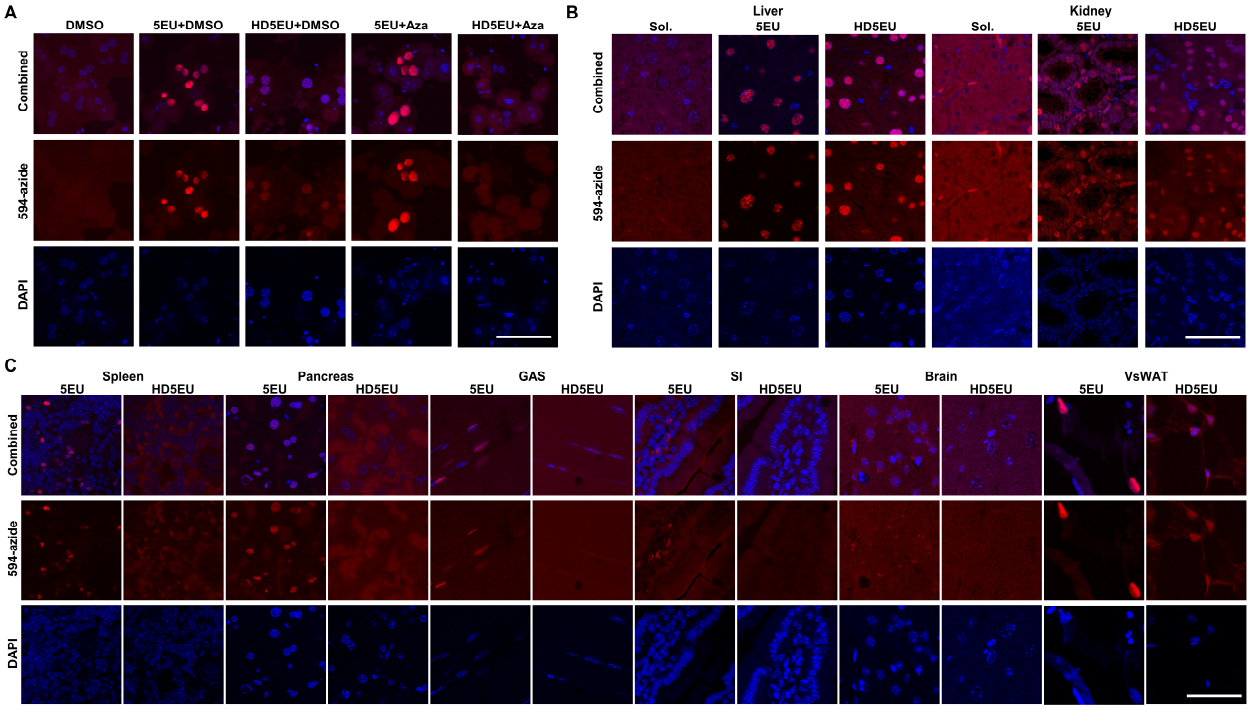

162

163 **Figure 2. Tissue specific staining evident with HD5EU is dependent on CYP3A4 activity.**
164 **A)** Primary hepatocytes demonstrate fluorescent nuclear staining of nascent RNA transcription
165 following 8 hours of 5EU and HD5EU treatment. Azamulin treatment hinders fluorescent nuclear
166 staining in HD5EU treated cells but not 5EU treated cells. 594-azide used for click-it staining. **B)**
167 Following 2 hours of HD5EU administration to mice, in-vivo fluorescent nuclear staining is
168 restricted to hepatocytes and epithelial cells in the kidney and absent from other tissue as evident
169 in panel C and supplementary figure 2. Sol. = solvent for HD5EU. **C)** A similar treatment with
170 5EU in-vivo results in fluorescent nuclear staining of cells in multiple tissue including; Spleen,
171 Pancreas, Muscle, Small Intestine, Brain and VsWAT. Consecutive injections did not change the
172 observed staining pattern as no tissue apart from liver and kidney demonstrated positive staining.
173 Scale Bar = 50µM. For negative controls see supplementary figure 2.

174

175 **Mass-Spectrometric validation and quantification of 5EU incorporation into RNA following**
176 **HD5EU treatment**

177 To validate that nuclear staining evident in-vitro and in-vivo following HD5EU treatment is indeed
178 indicative of 5EU incorporation into transcribing RNA, we adopted the mass-spectrometry method
179 described by **Su et. al [41]**. Using a column with a smaller inner diameter and lower flow rates to
180 improve the response of individual nucleotides, we were able to identify a wide range of
181 unmodified and modified nucleotides **(Sup. Table 1)**. 5EU (m/z 269.0768) was well separated
182 from the potential interfering 13C-Adenosine isotope (Adenosine m/z 268.1040, 13C-Adenosine
183 m/z 269.106541) in standard samples **(Figure 3a)**. Due to mass spectrometric settings all
184 nucleotides show a prominent in-source fragment, which corresponds to the neutral loss of the
185 ribose (**Figure 3b**, denoted as $[M-132+H]^+$).

186 Tandem mass spectrometry validated that 5EU is present in RNA extracted from the liver of
187 HD5EU treated mice **(Figure 3a-d)**. The main fragment at 20eV collision energy was the neutral
188 loss of ribose ($[M-132+H]^+$) consistent with the observed in-source fragment **(Figure 3b-c)**.
189 Further fragments of the remaining nucleoside fragment were observed under higher collision
190 energy of 40 eV **(Figure 3d)**. To quantify 5EU incorporation into RNA we used the prominent in-
191 source fragment of 5EU due to the low abundance of 5EU in biological samples, as this in-source
192 fragment was up to 3-5-fold higher than the intact molecule. In-vitro, Azamulin treatment of
193 primary hepatocytes inhibited HD5EU metabolism and incorporation into transcribing RNA
194 **(Figure 3e)**, in-line with observed fluorescent staining **(Figure 2a)**. In-vivo, we could detect and
195 quantify 5EU incorporation into both short (less than 200bp) and long RNA isolated from the liver
196 of HD5EU treated mice, 2 hours following the administration of the compound **(Figure 3f-g)**. 8h
197 following HD5EU administration 5EU was still detectable in long RNA (though it could not be
198 accurately quantified as it was below quantification limit), whilst only a moderate reduction was
199 detected in short RNA.

200 Taken together, these results confirm that HD5EU is metabolized in a CYP3A4 dependent manner
201 to 5EU, which is then incorporated into transcribing RNA.

202

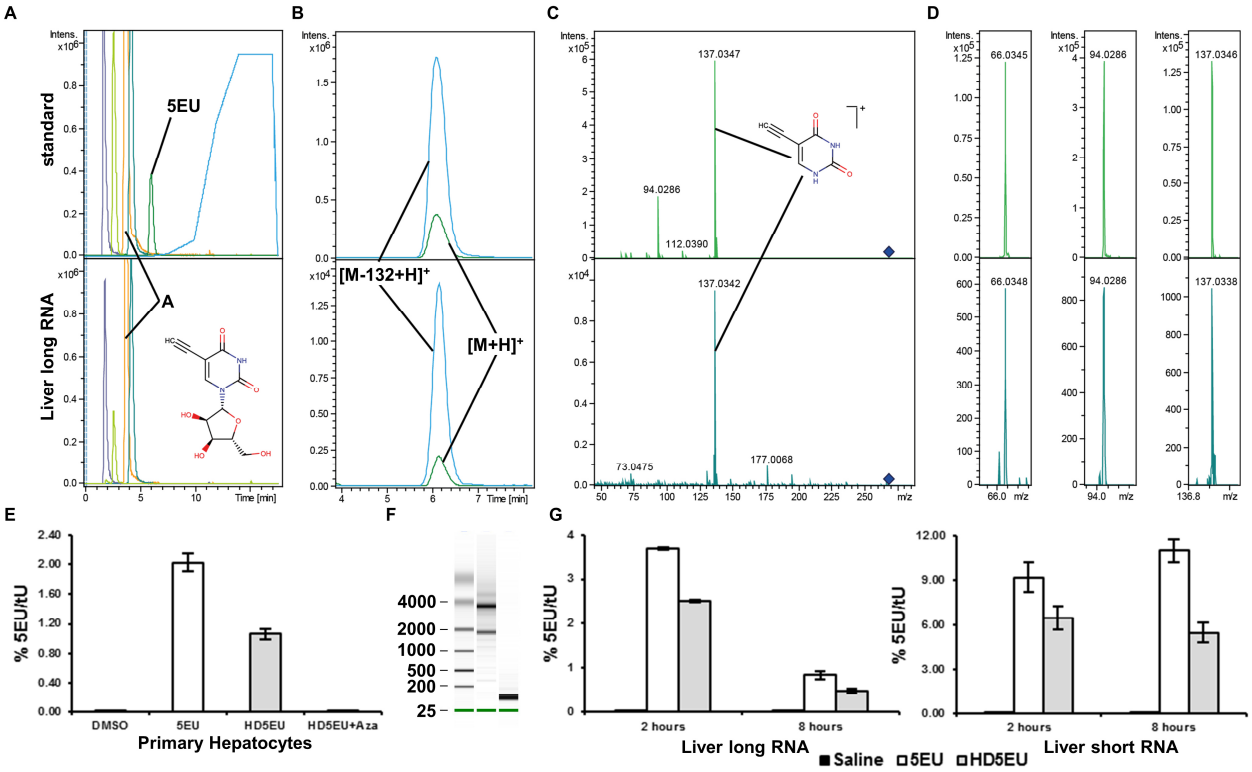

Figure 3. MS validation and quantification of 5EU in liver RNA of HD5EU treated mice. A) Extracted ion chromatograms from A, C, G, U and 5EU and gradient slope. **B)** Close up of extracted ion chromatograms of 5EU $[M+H]^+$ and 5EU in-source fragment $[M-132+H]^+$. **C)** Tandem MS spectra at 20 eV of standard and sample indicating main fragment $[M-132+H]^+$. **D)** Further fragments at 40eV used for identification of 5EU in RNA samples. **A-D** upper panels depict standard, lower panels depict liver long RNA from HD5EU treated mice. **E)** Relative quantification of 5EU in primary hepatocytes treated for 8h with the indicated compounds. Azamulin treatment inhibits CYP3A4 mediated HD5EU metabolism to 5EUMP and its subsequent incorporation into RNA. **F)** Bioanalyzer image depicting isolation of liver long and short RNA. **G)** Relative quantification of 5EU in liver derived long / small RNA following indicated time after 5EU / HD5EU administration to mice. Error bars indicated standard deviation calculated for 3 biological replicates.

Robustness and reproducibility of RNA precipitation.

2 hours following administration of HD5EU, 5EU-containing liver and kidney transcripts can be biotinylated and pulled-down for next generation sequencing. We persistently failed to generate any amplified libraries following pull-down of unlabeled RNA isolated from liver, plasma or

221 kidney of saline treated control mice **(Sup. Figure 3a-e)**. In addition, following a 2 hour treatment
222 with HD5EU we failed to generate libraries following biotinylation and pull-down from plasma
223 and from additional tissues of the HD5EU-treated mice, this in contrast to liver and kidney where
224 expected library amplicons were generated **(Sup. Figure 3a-e)**. This result was consistent for both
225 poly-A enriched and small RNA libraries and suggests biotinylation to be specific for 5EU
226 containing transcripts. Technical replicates of pull-down libraries demonstrated a high degree of
227 correlation between themselves, supporting the technical robustness and reproducibility of the
228 method **(Sup. Figure 3f,** spearman correlation coefficient = 0.95**)**.
229 To further assess the levels of non-specific RNA pull-down, we prepared a 10:1 mixture of non-
230 labeled small RNAs from *S. Cerevisiae* with labeled small RNAs derived from mouse liver.
231 Library construction and sequencing of this mixture following RNA pull-down demonstrated
232 highly effective depletion of yeast RNA compared to input **(Figure 4a)**. These results demonstrate
233 RNA pull-down to be highly selective to biotinylated RNA and non-specific RNA precipitation to
234 be extremely low to not detectable.
235
236 **RNA labelling in-vivo uncovers tissue architecture and stress induced transcriptional**
237 **reprogramming.**
238 We continued to examine if in-vivo labeling enriches for transcriptional programs of specific
239 cellular populations within complex tissues in-vivo, such as the proximal renal epithelial cells in
240 the kidney and hepatocytes in liver, and whether detection of environmentally induced
241 transcriptional reprogramming is possible. To this end we fed mice with high fat (**HFD**) or control
242 low fat (**LFD**) diets for two weeks. Following this acute HFD exposure, which is expected to alter
243 the transcriptional program in the liver [42], we administered HD5EU 2 hours before sacrificing.
244 We then continued to generate poly-A RNA libraries from kidney and liver input and pull-down
245 RNA.
246 Following mapping with the STAR aligner [43], transcript quantification using HTSeq-count and
247 differential pull-down analyses using the NOISeq package [44], we defined pulled-down
248 transcripts as those whose abundance can be estimated with a high degree of confidence to be at
249 least half of the abundance observed in input (i.e. at least 50% of the gene's transcripts are labeled
250 with a probability cut-off of 0.975) (**Figure 4b-g, Sup. table 2**).

251 In kidney, where proximal renal epithelial cells are labelled, GO annotation and gene set
252 enrichment analysis using Enrichr [45] demonstrated an enrichment for genes localized to the
253 brush boarder membrane, along with a few more general terms found enriched also in input such
254 as mitochondria, focal adhesion and genes specific to or highly expressed in the kidney **(Figure**
255 **4b-c, Sup. table 3)**. The brush boarder membrane in the kidney is a unique feature of proximal
256 renal epithelial cells [46], and among pulled-down transcripts, the Solute Carrier Family 9 member
257 A3 (Slc9a3) is one of its specific markers. Slc9a3 is the sodium–hydrogen antiporter 3, which is
258 highly expressed in the proximal tubule and allows active transport of sodium to the cell. Terms
259 uniquely enriched in genes depleted following pull-down include genes associated with ribosomal
260 function, genes specific to or highly expressed in CD34 positive cells, dendritic cells as well as
261 genes associated to neutrophil ficolin granules. CD34 positive cells are likely endothelial cells
262 found in glomeruli and blood vessels in both human and mice but absent from tubules [47, 48].
263 In liver, enrichment for identified liver targets of the nuclear receptors PPARA, LXR and RXR is
264 evident in both depleted and pulled-down transcripts. Pulled-down transcripts demonstrate
265 additional enrichment for identified liver targets of transcription factors such as Foxo1, Clock and
266 Nucks1 and for transcripts localizing to nuclear speckles and nucleoli **(Figure 4d-e, Sup. table 4)**.
267 LXR and RXR are implicated in lipid metabolism and heterodimerize to regulate gene expression.
268 Their transcriptional upregulation is associated with increased hepatic lipogenesis [49]. PPARA
269 instead, binds long chain free fatty acids and is a central regulator of lipid metabolism. It
270 heterodimerizes with RXR or LXR to regulate mitochondrial and peroxisomal fatty acid oxidation
271 [50-52].
272 Published single-cell sequencing from kidney [53] and liver [54] supports depletion of genes
273 associated with irrelevant cell types in both organs. Using published single-cell data, we compared
274 the top ranking genes defined in each study to be cluster specific markers to our pull-down
275 enrichment results. In kidney, we find the majority of cluster markers to be depleted following
276 pull-down of kidney poly-A RNA, apart from a small subset of markers for proximal tubule cells
277 **(Figure 4f)**. In liver, this trend continued and from the list of cluster specific markers, 80% of
278 those identified as enriched following liver poly-A RNA pull-down were defined as markers of
279 hepatocyte clusters.

280 Taken together these results support specific labelling of renal proximal tubule epithelial cells in
281 the kidney and of hepatocytes in the liver, with enrichment of their transcriptomes in pulled-down
282 RNA and specific depletion for genes associated with other cell types found in these organs.
283 To assess the feasibility of detecting dynamic transcriptional responses using iTag-RNA, we
284 examined whether diet-induced transcriptional reprogramming can be identified in pulled-down
285 poly-A RNA, and to what extent it reflects transcriptional changes observed in whole-tissue input
286 RNA. Differential gene expression analyses using the DEseq package [55] revealed a substantial
287 overlap between diet induced transcriptional reprogramming in the liver as observed in input
288 mRNA to transcriptional reprogramming observed in pull-down libraries **(Figure 4g, Sup. table**
289 **5**). Though the total amount of differentially expressed genes **(DEG)** was roughly 4 fold lower in
290 pull-down vs. input libraries (157 vs. 636 DEG, with an FDR cutoff of less than 0.05 and absolute
291 log2 fold change greater than 1), a 61% overlap (96 DEG) between the two sample sets was
292 detected. This overlap is much higher than expected by chance (chi test <0.0001). Diet induced
293 DEG in both input and pull-down liver RNA demonstrated a significant enrichment for genes
294 regulated by PPARA, LXR and RXR **(Figure 4h and Sup. Table 7**).
295 As opposed to liver, diet-induced differential expression in the kidney was limited to 108
296 transcripts in input poly-A RNA enriched for mitochondrial and ribosomal proteins, whilst pulled-
297 down RNA demonstrated no transcriptional reprograming **(Figure 4i-j, Sup. table 6-7).** These
298 findings may reflect the more complex cellular composition of the kidney and a lack of
299 transcriptional reprogramming in proximal renal epithelial cells.
300 Taken together, these results provide a proof-of-concept that iTAG-RNA allows isolation of cell-
301 type specific transcriptional responses to environmental challenges. Importantly, with no need for
302 the disruption of the tissue architecture or interference with the cellular microenvironment.
303

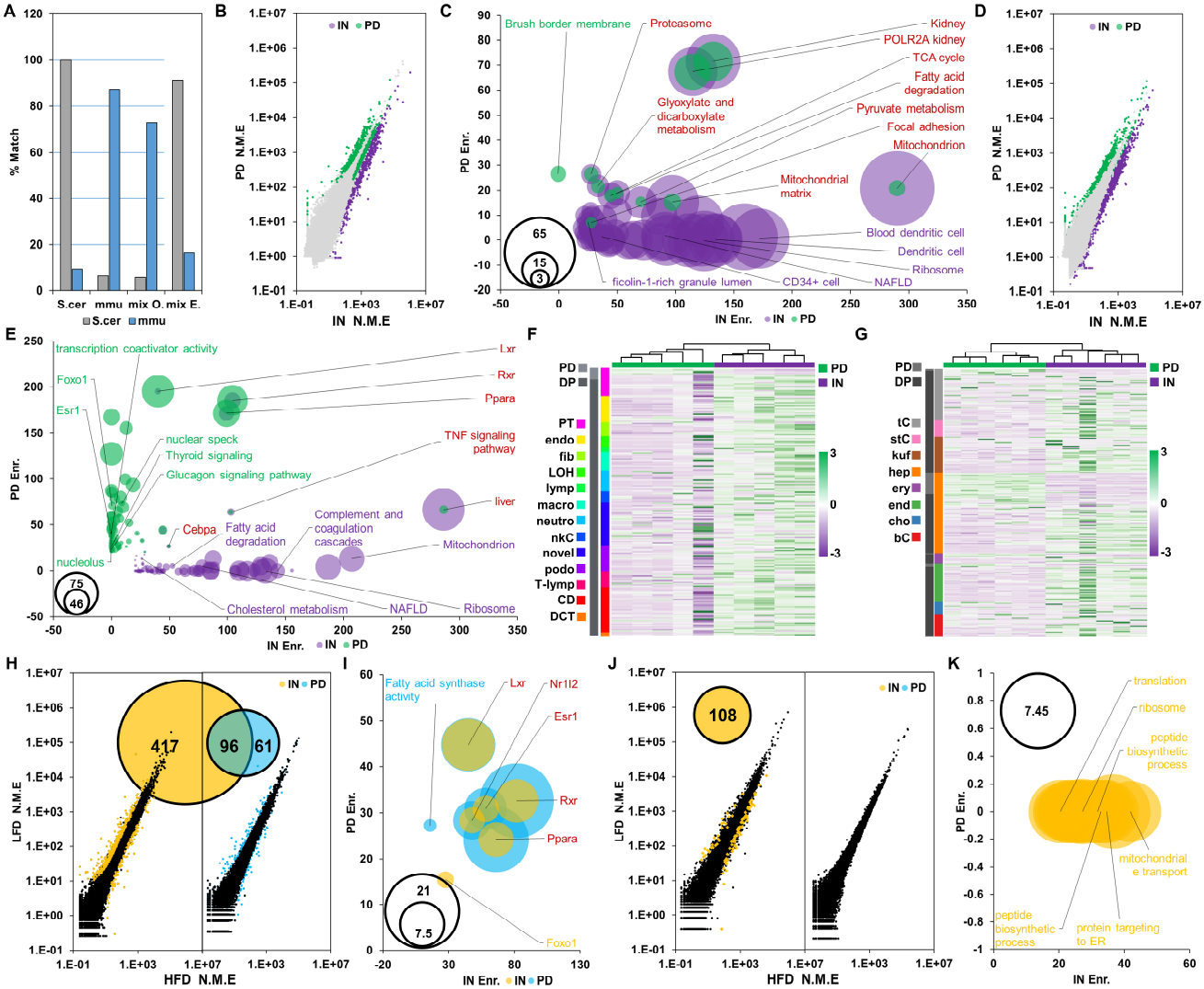

Figure 4. mRNA pull-down enriches for specific cell populations in vivo. A) Pull-down of a 10:1 mixture of unlabeled yeast RNA with labeled RNA from mouse liver specifically depletes unlabeled yeast RNA (gray) whilst enriching for the labelled mouse RNA (blue). Compare observed (mix O.) ratios of genomic alignment to expected ratios (mix E.) **B)** Scatter plot visualizing pulled-down (green) and depleted (purple) poly-A RNA from mouse kidney. **C)** GO and gene set enrichment analysis for pulled-down (green) and depleted (purple) protein coding transcripts in kidney. An enrichment for brush boarder membrane proteins, a unique feature in the kidney of proximal epithelial cells, is evident in pulled-down transcripts. Bubble size proportional to $-\log_{10}$ of adj. PV. **D)** Scatter plot visualizing labelled pulled-down (green) and depleted (purple) poly-A RNA from mouse Liver. **E)** GO and gene set enrichment analysis for pulled-down (green) and depleted (purple) protein coding transcripts in liver. Bubble size proportional to $-\log_{10}$ of adj.

316 PV. **F)** Markers for various cell types found in the kidney and their relative expression in our input
317 and pull-down poly-A RNA libraries. Markers adopted from Park J. et. al. [53]. PT = proximal
318 tubule; endo = endothelial cells; fib = fibroblasts; LOH = Loop of Henle; lymp = lymphocytes;
319 macro = macrophages; neutro = neutrophils; nkC = natural killer cells; novel = novel cell type;
320 podo = podocytes; T-lymp = T-lymphocytes; CD = collecting duct; DCT = distal convoluted
321 tubule. PD = pulled-down, DP = depleted. IN = Input. **G)** Markers for various cell types found in
322 the liver and their relative expression in our input and pull-down poly-A RNA libraries. tC = t-
323 cells; stC = stellate cells; kuf = kuffer cells; hep = hepatocytes; ery = erythrocytes; end =
324 endothelial cells; cho = cholangiocytes; bC = b-cells. Markers adopted from MacParland et. al.
325 [54]. PD = pulled-down, DP = depleted. IN = Input. **H)** Venn diagram demonstrating the overlap
326 between differentially expressed genes in input liver mRNA (orange) and pull-down liver mRNA
327 (Blue) with the corresponding scatterplot. HFD normalized mean expression on the X-axis, LFD
328 normalized mean expression on the Y-axis. **I)** Differentially expressed genes in input kidney
329 mRNA (orange) with the corresponding scatterplot. HFD normalized mean expression on the X-
330 axis, LFD normalized mean expression on the Y-axis. No DEG detected in pull-down mRNA.
331 Bubble size proportional to $-\log_{10}$ of adj. PV. **J)** GO and gene set enrichment analysis for dietary
332 induced differentially expressed protein coding genes identified in pull-down (blue) and input
333 (orange) liver libraries. **K)** GO and gene set enrichment analysis for dietary induced differentially
334 expressed protein coding genes identified in input kidney libraries. Bubble size proportional to –
335 $\log_{10}$ of adj. PV.
336

337 **Hepatocyte derived ccfRNA are detected in Plasma**

338 Given the observed hepatic transcriptional reprogramming following a HFD challenge, we
339 examined whether we can detect labeled hepatocyte derived plasma ccfRNAs, and if the profile of
340 these secreted transcripts changes in response to the dietary challenge. Plasma isolated ccfRNAs
341 are predominantly short / fragmented RNA transcripts with a bi-modal distribution and a major
342 peak smaller than 200bp ([56] **and sup figure 3g**). As already described, with a single dose of
343 HD5EU 2 hours before blood collection we failed to generate libraries from plasma ccfRNA
344 following biotinylation and pull-down. However, with multiple doses of HD5EU administration
345 6, 4 and 2 hours before blood collection, we were able to generate small RNA libraries following
346 pull-down of plasma ccfRNAs.

347 Multiple short RNAs were pulled-down in both liver and plasma under HFD and LFD. (**Figure**
348 **5a,** 459/992 for HFD and 234/700 for LFD). This co-occurrence rate is greater than expected by
349 chance for HFD and LFD **(Figure 5a,** P.V calculated using the SuperExactTest package in R [57],
350 Fold enrichment = HFD: 2.7; LFD = 1.8; P.V. = HFD: 4.3e-104; LFD = 6.42e-21). The identity of
351 pulled-down plasma ccfRNAs varied between dietary challenges **(Figure 5b and Sup. tables 8-**
352 **10)**, with multiple reads found enriched only under a specific dietary challenge, suggesting that
353 liver secreted ccfRNAs indeed change with dietary interventions.
354 Various biotypes are identified in pulled-down liver and plasma short RNA libraries, with the
355 relative proportion of pulled-down transcripts varying between the two. tRNAs, mitochondrial
356 tRNAs and mitochondrial genes are found to be overly represented in pull-down RNA from plasma
357 relative to liver (**Figure 5c**). This result suggests that the majority of mitochondrial transcripts
358 found in plasma originate predominantly in the liver.
359 Additional support in favor of the hepatic origin of plasma labeled transcripts can be found in
360 fragments originating from protein coding genes. These protein coding fragments demonstrate a
361 significant enrichment for liver specific and highly expressed genes, whilst transcripts
362 constitutively depleted in pull-down RNA demonstrate an enrichment for bone marrow specific
363 protein coding fragments, genes related to hematopoietic differentiation and genes specific to
364 neutrophil function. **(Figure 5d and sup. table 11)**. This result may suggests that the
365 hematopoietic system is one of the major contributors of circulating RNAs. HFD and LFD specific
366 pulled-down protein coding transcripts demonstrate differential enrichment for annotations
367 including adipocytokine signaling and mitochondrial electron transport respectively (**Figure 5e**).
368 The significant enrichment found for liver specific protein coding genes among pulled-down
369 transcripts supports the hypothesis that pulled-down ccfRNA transcripts originate in hepatocytes,
370 where Cyp3a4 expression metabolizes HD5EU to 5EU, allowing its incorporation into nascent
371 transcribing RNA.
372

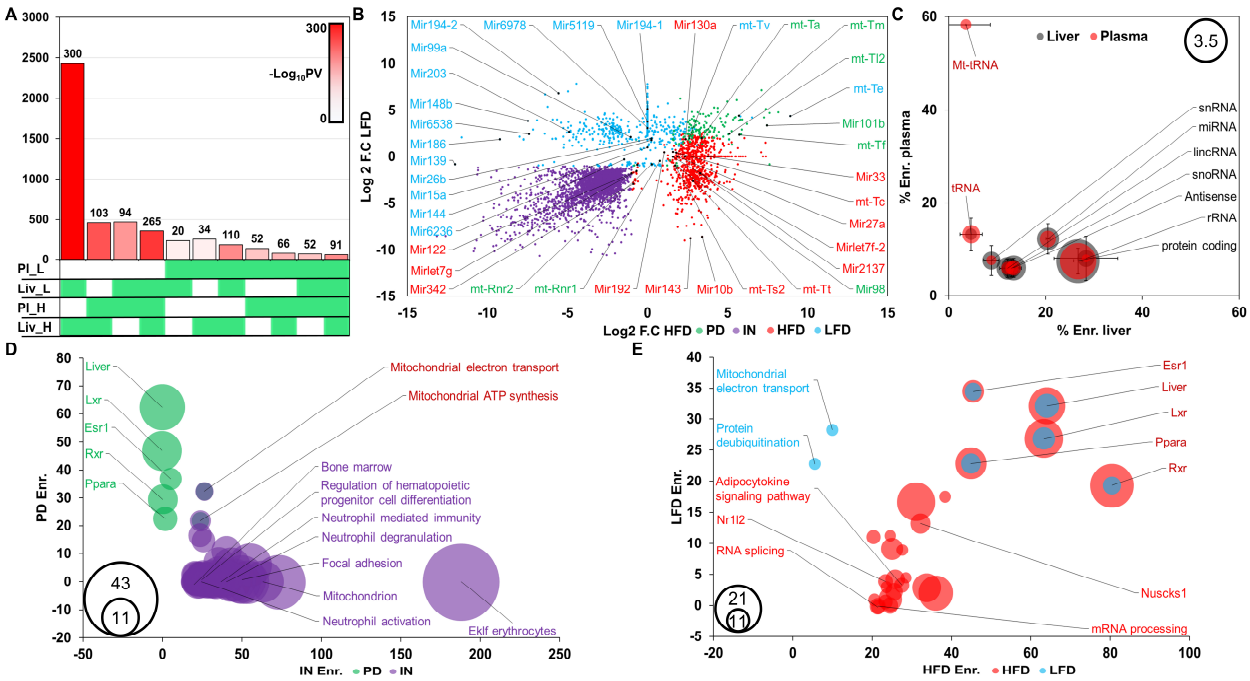

Figure 5. Identification of hepatocyte secreted circulating transcripts in Plasma. A) Overlap between pulled-down small RNA transcripts in liver and plasma under HFD and LFD challenge. Number of transcripts per overlap indicated in the y-axis. Color corresponds to $-\log_{10}$ of calculated P.V and is annotated in the chart. Gene sets included in each comparison are indicated in green. **B)** Scatter plot annotating selected miRNAs and mt-tRNAs identified as pulled-down in circulating plasma RNA under HFD and LFD conditions. Transcripts are either depleted following pull-down regardless of dietary regime (purple), pulled-down regardless of dietary regime (green) or pulled-down under HFD (red) or LFD (blue) dietary regimes only. **C)** Bubble plot representing the relative percentage of pulled-down transcripts per biotype in liver and plasma libraries, averaged across HFD and LFD regimes. Bubble size represents log10 of actual number of transcripts per bio-type. Error bars for standard deviation between sets. **D)** Bubble plot of GO and gene set enrichment analysis for constitutively pulled-down (green) and depleted (purple) cell-free circulating transcripts. Bubble size proportional to $-\log_{10}$ of adj. PV. **E)** Bubble plot of GO and gene set enrichment analysis for cell-free circulating transcripts pulled-down in HFD (red) or LFD (blue). Bubble size proportional to $-\log_{10}$ of adj. PV.

Hepatic derived ccfRNA are found in visceral white adipose tissue where they contribute to the small RNA pool and potentially regulate lipid storage

392 In worms, plants and prokaryotes, extracellular RNA signaling was described to modulate
393 host/pathogen interactions and to orchestrate an adaptive response to environmental stimuli [58-
394 60], and demonstrated the idea that biological systems can exist as holobionts characterized by
395 continuous exchange of genetic (DNA, RNA) material. In mammals, RNA-based intercellular
396 signaling has been described in several settings [4, 9, 12, 61-63], using mostly in-vitro systems or
397 ectopic administration of RNAs to demonstrate RNA transfer and signal transduction. Little is
398 known on the extent of RNA transfer in-vivo and on the role it may play in physiological settings.
399 Two weeks of high-fat diet feeding are sufficient to impair metabolic homeostasis [64], and induce
400 morpho-functional alterations in both liver and visceral adipose tissue [64]. Given the central role
401 liver and adipose tissue play in metabolic control [65], and existing evidence suggesting RNA-
402 based signaling between the tissues [12], we used iTAG-RNA to identify diet-sensitive RNA-
403 based liver-to-adipose signals.
404 The number of transcripts found to be enriched following pull-down in liver, plasma and VsWAT
405 was 9.7 folds greater than expected by chance for HFD and 6.8 folds greater than expected for
406 LFD (HFD: 264/27, PV=6.34e-180 ; LFD: 116/17, PV = 3.7e-59 as calculated using the
407 SuperExactTest package in R [57]) (**Figure 6a Sup tables 8-10**). Focusing on identified hepatic
408 transcribed plasma ccfRNAs, multiple small RNAs could be enriched for in VsWAT. These
409 include miRNAs such as mir-33, mir-10b and mir-130a, in addition to mt-tRNAs (**Figure 6b**).
410 Among experimentally validated targets of the identified miRNAs (as annotated by miRTarBase
411 [66]), an enrichment is found for proteins associated with the GO term negative regulation of lipid
412 storage (GO:0010888, adj. P.V. = 0.0078, enrichment score = 26.68) such as Abca1, Ppara and
413 Pparg which are regulated by mir-33 [23, 24], mir-10b [25] and mir-130a [26, 67] respectively.
414 Mir-33 is also an identified regulator of the Srebp family of transcription factors that are central
415 in cholesterol and fatty acid synthesis [68, 69] and is in fact encoded within the intron of Srebf2.
416 Total RNA sequencing of VsWAT identified 100 genes to be differentially expressed following
417 acute HFD feeding (28 upregulated / 72 downregulated, **Sup table 12**). As expected given the
418 increased dietary intake of free fatty acids following HFD feeding, downregulation of Srebf1 and
419 of several target genes involved in fatty acid biosynthesis such as FasN, Acaca, and Scd2 is evident
420 (**Figure 6c-d**).
421 Based on the described literature on intercellular RNA signaling, two main effects can be
422 envisaged for the transfer of ccfRNAs between tissues: 1. Direct alterations to a cell's

423 transcriptomic pool via introduction of novel regulatory RNAs, and 2. Modulation of existing
424 intracellular pools of regulatory RNAs. Both scenarios can have varying degrees of functional
425 consequences on the transcriptional and physiological responses of the recipient cell.
426 To explore these two possibilities, we looked at the expression levels in VsWAT of the identified
427 miRNAs. Paradoxically, both small RNA-Seq and qRT-PCR (Fig.6e) confirmed that rather than
428 upregulation of these miRNAs in VsWAT following HFD, no change or a moderate
429 downregulation in their levels is evident. This result most likely reflects a HFD-induced
430 downregulation of the endogenously transcribed adipocyte miRNAs and suggests that the transfer
431 of exogenous hepatic derived miRNAs buffers the downregulation of the adipocyte transcribed
432 miRNAs. Indeed upon acute HFD feeding and in keeping with mir-130a downregulation and
433 published results, Pparg protein but not transcript levels are modestly upregulated (**Figure 6d, f**).
434 All together, these results show – for the first time – transfer of regulatory RNAs from hepatocytes
435 to adipocytes in response to acute dietary challenge and suggest a potential function in buffering a
436 cell's transcriptional and physiological responses.

437

438 Figure 6. Plasma ccfRNAs can be detected in VsWAT. A) Venn diagram demonstrating the
439 overlap between pulled-down transcripts in expression sets from liver plasma and VsWAT for
440 HFD and LFD (Blue = Liver; Red = Plasma; Yellow = VsWAT). B) miRNAs and mt-tRNAs that
441 are pulled-down in both plasma and VsWAT (Red = HFD; Blue = LFD). C) Volcano plot
442 demonstrating DEG in total RNA sequencing of VsWAT following 2 weeks of HFD or LFD
443 challenge. Red – downregulated in HFD, Green – Upregulated in HFD. D) qRT-PCR estimations
444 for differential expression of Pparg and Fasn in VsWAT. # = significant fold change, n=3. E) qRT-
445 PCR estimations for differential expression of selected miRNAs. # = significant fold change, n=3.
446 F) Western blot for Pparg, modest upregulation of Pparg levels is evident following 2 weeks of
447 HFD. G) Depiction of small RNA transfer between liver and adipose tissue. H) A model suggesting
448 that the small RNA pool within a cell results from a balance between transcription and degradation
449 on the one hand and influx and efflux on the other.

450

451 **Discussion**

452 In this work we present **iTAG-RNA**, a novel method for targeted in-vivo labelling of global RNA
453 transcription, and use it to identify hepatocyte secreted ccfRNA and their uptake by adipose tissue
454 in-vivo. iTAG-RNA allows labelling of total RNA transcripts in-vivo using two main components:
455 **HD5EU**, a newly designed small molecule that serves as a metabolite for the human CYP3A4
456 enzyme; and **an existing humanized transgenic mouse model** expressing the human CYP3A4
457 enzyme under a modified APOE promoter **(Figure 1)**. CYP3A4 catalyzes the oxidative cleavage
458 of an aryl group of the HD5EU molecule, which in turn undergoes spontaneous beta elimination
459 to produce a bio-available 5EU-monophosphate. The existing transgenic mouse model allows in-
460 vivo labelling of hepatocytes and kidney proximal renal epithelial cells **(Figure 2),** as the tissue
461 expression pattern of the enzyme dictates the site of the small molecule's metabolism and
462 subsequent RNA labeling. To validate the specificity of HD5EU metabolism, we demonstrate that
463 HD5EU is indeed metabolized in a CYP3A4 dependent manner to 5EU-monophosphate. 5EU is
464 then incorporated in place of uridine into transcribing RNA **(Figure 2-3)** and allows highly
465 selective RNA precipitation and sequencing of labeled RNAs (**Sup. Figure 3 and Figure 4a**).
466 Development of new transgenic models would allow for labeling of multiple tissues of choice.
467 Administration of HD5EU allows enrichment for the transcriptional program of proximal renal
468 epithelial cells and hepatocytes in-situ without disruption of the kidney or liver architecture
469 **(Figure 4b-g)**. In addition, environmentally induced transcriptional reprogramming is evident
470 following labelling (**Figure 4h-k**). As opposed to recently described methods [14, 17, 20, 22] and
471 in keeping with the literature where POLI, POLII and POLIII are demonstrated to incorporate 5EU
472 [27], mRNA and small RNAs of various types including rRNA, tRNA and miRNA are found to
473 be labeled and enriched in pulled-down RNA.
474 Critically, and uniquely to iTag-RNA, we are also able to enrich for liver derived plasma ccfRNA
475 following an administration of multiple doses of HD5EU **(Figure 5)**. Pulled-down plasma
476 ccfRNAs demonstrate an enrichment for liver derived RNA fragments of protein-coding genes,
477 whilst depleted transcripts demonstrate an enrichment for annotation relating to function and
478 differentiation of the hematopoietic system. Apart from fragments of protein coding genes, liver
479 secreted ccfRNA include various small RNA transcripts such as miRNA, mt-tRNAs and tRNAs.
480 Given the evident enrichment for mitochondrial transcripts following pull-down, our results

481 suggest that hepatocytes are the main source of mitochondrially encoded ccfRNA transcripts in
482 plasma. The functional significance of these tRNA fragments is unclear, but several studies have
483 suggested tRNAs and tRNA fragments can mediate cellular signaling, and that the overall tRNA
484 pool and composition within a cell has functional significance [70].
485 We continued to explore the possibility that ccfRNAs are taken up by tissues in-vivo to mediate
486 cell-to-cell communication. Focusing on VsWAT we pulled-down and amplified labeled RNA,
487 again following multiple doses of HD5EU **(Figure 6a)**. The transcripts we identified as labeled in
488 VsWAT demonstrated a greater overlap than expected by chance with labeled plasma ccfRNAs or
489 indeed with labeled transcripts in the liver, supporting their hepatic transcriptional origin. These
490 transcripts including miRNAs and mt-tRNAs **(Figure 6b),** with the identified miRNAs implicated
491 in post-transcriptional regulation of proteins involved in lipid, cholesterol and fatty acid pathways.
492 Together our results directly demonstrate for the first time, in-vivo transfer of a large variety of
493 RNAs including miRNAs between hepatocytes and visceral adipose tissue (**Figure 6g**), with the
494 identity of transferred RNAs varying following an acute dietary challenge. In light of the observed
495 diversity and scope of RNA transfer between hepatocytes and adipocytes, our results suggest that
496 the pool of small RNAs in a cell in-vivo results from a balance not only between transcription and
497 degradation, but also influx and efflux of small RNAs from the extracellular environment (**Figure**
498 **6h**), with the latter serving as a buffering mechanism for transcriptional and physiological
499 responses in target cells.
500 To date, the majority of potential ccfRNA biomarkers associated with liver pathologies have been
501 miRNAs [71]. Our findings suggest that fragments of protein coding genes together with
502 mitochondrial tRNAs and mitochondria encoded transcripts can also serve as useful biomarkers
503 for hepatic function. Development of additional genetic models similar to the one used can allow
504 for better transcriptional characterization of distinct cell populations in-vivo, with the added
505 benefit of labelling endogenous ccfRNAs in-vivo. Lastly, HD5EU may prove beneficial in clinical
506 settings. As metabolic activation of HD5EU requires the human Cyp3a4 enzyme, whose
507 expression under physiological conditions is largely limited to the liver (The human protein atlas.
508 2019. CYP3A4. [ONLINE] Available at: https://www.proteinatlas.org/ENSG00000160868-
509 CYP3A4/tissue/primary+data **[72]**), administration of this small molecule to humans may
510 constitute a novel diagnostic tool allowing assessment of hepatic function by means of a liquid
511 biopsy.

512

513 **Methods:**

514 *Mice handling:*

515 Mice were purchased from Taconic (Taconic USA). All mice were kept in a SPF facility in
516 accordance with the Bavarian Animal law. Mice were fed with a chow / high fat diet / low fat diet
517 as indicated (Rodent Diet with 60 kcal% from fat - Research Diet D12492i, Rodent Diet with 10
518 kcal% from fat – Research Diet D12450B). 5EU (7848.2, Carl Roth) was solubilized in saline
519 0.9% NaCl, HD5EU in a 25 % PEG-400, 5% DMSO saline solution. Compounds were
520 administered intraperitoneally at a dose of 0.15 / $0.3_{mg/g}$ in a total volume of 200µl. First
521 administration was always carried out at ZG-3 to avoid circadian effects. For blood and organ
522 collection, mice were terminally anesthetized with Ketamin/Xylazine at indicated times following
523 drug administration. Heart puncture was performed to collect blood in EDTA coated syringes.
524 Blood was centrifuged at 4.8K rpm for 10' followed by 12K rpm at 20' and filtration through a
525 22uM PES filter (PA59.1, Carl Roth). For isolation of primary hepatocytes, mice were anesthetized
526 and liver perfused through the vena cava with Gibco's liver perfusion buffer (17701-038, Gibco)
527 and liver digestion buffer (17703-034, Gibco) in accordance with manufacturer's instructions.

528

529 *Cell culture:*

530 Isolated primary hepatocytes were counted using the countess automated cell counter (C10227,
531 invitrogen), and plated to a density of 75k/Cm^2 on Geltrex (A1413201, ThermoFisher) coated
532 coverslips (200 µg/cm^2) in Williams' Medium E (A12176, Gibco) supplemented with Gibco's
533 Primary Hepatocyte Maintenance Supplements (CM4000, Gibco). 24 hours following plating,
534 cells were treated with 1mM of 5EU or HD5EU for 8 hours. Azamulin (SML0485, Sigma Aldrich)
535 was added at a concentration of 20µM for 30 minutes before addition of indicated compounds to
536 a final concentration of 10µM for the length of the treatment.

537

538 *Tissue processing and imaging*

539 Tissues were fixed in a neutral buffered 10% formalin solution (HT501128, Sigma) for 48 hours
540 before dehydration and embedding in paraffin in accordance with published protocols. 4µm
541 sections were cut on a Leica microtome (RM2165, Institute of Experimental Genetics), rehydrated
542 and stained using the Click-iT™ RNA Alexa Fluor™ 594 Imaging Kit (C10330, ThermoFisher)

543 in accordance with manufacturer's instructions. Mounting was done with Vectashield hardset
544 antifade mounting medium with DAPI (H-1500, Vector Laboratories). Imagining was done using
545 a Laser Scanning Confocal Microscope (Olympus Fluoview 1200, Institute for Diabetes and
546 Cancer, Neuherberg, Germany) equipped with an Olympus UPlanSApo 60x 1.35 Oil immersion
547 objective.
548
549 *Western Blot*
550 Tissues were homogenized using a Miltenyi gentleMACS Dissociator (Miltenyi biotec) in RIPA
551 buffer supplemented with protease (S8820, Sigma Aldrich) and phosphatase (88667, Thermo
552 Fisher) inhibitors. Protein concentration was measured using a standard Bradford assay reagent
553 (B6916, Sigma Aldrich).40µg total protein were loaded per samples on a pre-cast gradient 4-12%
554 gel (NW04120, Invitrogen). Proteins were transferred to a PVDF membrane (ISEQ00010, Merck
555 Millipore) blocked and blotted using the iBind system (SLF1020, Invitrogen) with primary anti-
556 CYP3A4 (MA5-17064, Thermo Fisher), anti-Phospho-p53 S392 (#9281, cell signaling), anti-
557 total-p53 (#2524, cell signaling), anti-cleaved Caspase-3 (ab214430, abcam) , anti-total Caspase-
558 3 (#ab184787, abcam), anti-pparg (MA5-14889, Thermo Fisher), anti-histone H3 (4499s, cell
559 signalling) and anti-HSP90 (SC-7949, Santa-Cruz), and secondary IgG HRP (7076 and 7074, Cell
560 Signaling)
561
562 *RNA extraction, qRT-PCR, pull-down and library construction.*
563 Plasma RNA was extracted using TRI Reagent BD (T3809, Sigma Aldrich), in accordance with
564 manufacturer's instructions. RNA from tissues was extracted using NucleoZOL (740404.200,
565 Macherey-Nagel) reagent, in accordance with manufacturer's instructions. For qRT-PCR, reverse
566 transcription was conducted using the high-Capacity cDNA Reverse Transcription Kit (4368814,
567 Applied Biosystems), in accordance with the manufacturer's instructions. Real-time was carried
568 out on a quant-studio 6 flex (applied biosystems) with SYBR Green PCR Master Mix (#4309155
569 applied biosystems) and primers; hCyp3-F: TTGGCATGAGGTTTGCTCTC; hCyp3-R:
570 ACAACGGGTTTTTCTGGTTG; Pparg-F: AGATTCTCCTGTTGACCCAGAG; Pparg-R:
571 AGCTGATTCCGAAGTTGGTG; Fasn-F: CTGCTGTTGGAAGTCAGCTATG; Fasn-R:
572 ATGCCTCTGAACCACTCACAC; Actin-F: CACAGCTTCTTTGCAGCTCCT; Actin-R:
573 CAGCAGTGCAATGTTAAAAGG; qRT-PCR for miRNAs was conducted as previously

574 described [73] and primers designed with miRprimer2 [74]. miR-7f-5p-F:
575 CGCAGTGAGGTAGTAGATTG; miR-7f-5p-R: CAGGTCCAGTTTTTTTTTTTTTTAAC;
576 miR-130a-3p-F: CAGCAGTGCAATGTTAAAAGG; miR-130a-3p-R:
577 CAGGTCCAGTTTTTTTTTTTTTTATG; miR-33-5p-F: CGCAGGTGCATTGTAGT; miR-
578 33-5p-F:GTCCAGTTTTTTTTTTTTTTTGCAAT; miR-10b-5p-F
579 CAGTACCCTGTAGAACCGA; miR-10b-5p-R:GGTCCAGTTTTTTTTTTTTTTTCAG; Pull-
580 down of 5EU labeled RNA was done using the Click-it Nascent RNA Capture Kit (C10365,
581 Thermo Fisher). 10µg total / small RNA was used as input from tissues, 200ng plasma RNA was
582 used as input for RNA pull-down from blood. RNA was used as template for library construction
583 using the CATS mRNA/small RNA kit (C05010043 and C05010040, Diagenode) with slight
584 modifications to protocol i.e.; Poly-A selection and RNA fragmentation were performed before
585 biotinylation and pull-down of 5EU. 14 cycles of amplification for RNA from tissues, 20 for RNA
586 from blood. 10ng of RNA was used for Input. For MS analysis, 10µg long / short RNA was used.
587 RNA was digested as described in Sue et. al. [41].
588
589 *UPLC-UHR-ToF-MS analysis*
590 Mass spectrometric analysis of nucleotides from RNA was performed on a Waters Acquity UPLC
591 (Waters, Eschborn, Germany) coupled to a Bruker maXis UHR-ToF-MS (Bruker Daltonic,
592 Bremen, Germany). Separation was performed on a Thermo Hypersil Gold column (150 x 1.0 mm,
593 3 µm, 25003-151030, Thermo Fisher) using a multistep gradient with 100% water and 100% ACN,
594 both with 0.1% formic acid. Gradient conditions were as followed: 0-6 min 0% B, 6-7.65 min
595 linear increase to 1% B, 7.65 to 10 min linear increase to 6% B, 10 to 12 min linear increase to
596 50% B, 12 to 14 min linear increase to 75% B, 14 to 17 min isocratic hold of 75% B, 17 to 17.5
597 min return to initial conditions. Column temperature was 36°C and flow rate was set to 0.09
598 ml/min. Before each run the column was re-equilibrated for 3 minutes with starting conditions.
599 High mass accuracy was achieved by infusion of 1:4 diluted ESI low concentration tune mix
600 (Agilent Technologies, Waldbronn, Germany) at the start of each chromatographic run. Each
601 analysis was internally recalibrated using the tune mix peak at the beginning of the chromatogram
602 using a custom VB script within Bruker DataAnalysis 4.0 (Bruker Daltonic, Bremen, Germany).
603 Quantitative analysis was performed in Bruker QuantAnalysis 4.0 (Bruker Daltonic, Bremen,
604 Germany). High Resolution-Extracted Ion Chromatograms (HR-EICs) were created around each

605 precursor mass +/- 0.005 Da. Chromatograms were smoothed and peak areas were used for
606 quantification. In case of 5EU additional quantification was performed on a validated in-source
607 fragment $[M-132+H]^+$.
608
609 *Bioinformatic analysis*
610 RNA Libraries were sequenced on an Illumina HiSeq 2500 instrument (**IGA Technology Services**
611 **Srl, Italy**) at 75bp single-ended**.** Adaptors were trimmed in accordance with the CATS sequencing
612 kit manual. Reads were aligned to the mouse mm10 genome using the STAR aligner [43] and a
613 reference transcript gtf file from ensamble modified to contain tRNA transcripts as annotated by
614 GtRNAdb [75].
615 For the detection of differentially regulated genes between HFD and LFD the Deseq2 package was
616 used [55]. Pull-down enrichment analysis was conducted using the NOISeq package. Transcripts
617 with expression values smaller than a cpm of 1 and a coefficient of variation greater than 300 were
618 filtered out prior to tmm normalization and enrichment analysis. GO and gene set enrichment was
619 calculated using the Enrichr tool [45].
620
621 **Conflict of interest**
622 The authors declare no conflict of interest.
623
624 **Acknowledgments**
625 We would like to thank Dr. Julia Calzada-Wack, Jacqueline Mueller and Marion Fisch for their
626 kind assistance with tissue processing and sectioning. We thank Dr. Anja Zeigerer for access to
627 and assistance with the confocal microscope. This work has been supported by the German
628 Diabetes Research Center (DZD NEXT Grant 2019) to T.R., and by the ERC Recognition Award
629 from the Helmholtz Research Center Munich to T.R. The authors thank the Helmholtz Association
630 and the German Diabetes Research Center for funding the positions of G.R., D.J., L.M., S.F., T.A.
631 and T.R.
632
633 **Author contributions**
634 Conceptualization D.J.; Methodology D.J. and W.M.; Investigation D.J., L.M., G.R., A.T., S.F.
635 and W.M.; Writing – Original Draft D.J., W.M., and T.R.; Writing – Review & Editing D.J.,

H.A.M, W.M. and T.R.; Funding Acquisition H.A.M and T.R.; Resources; H.A.M, W.M. and T.R.; Supervision T.R.

Supplementary figures:

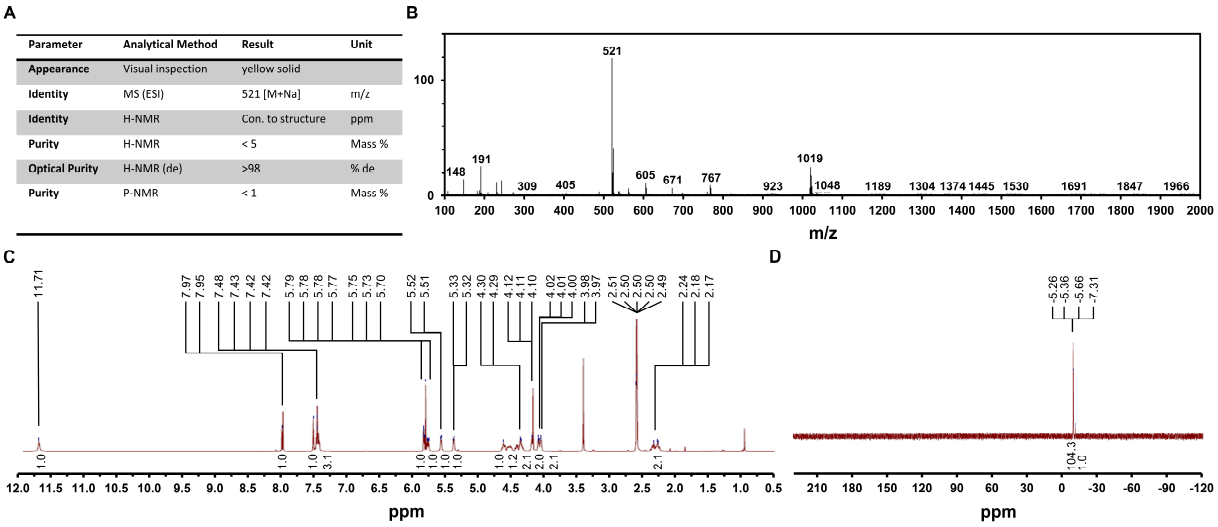

Parameter	Analytical Method	Result	Unit
Appearance	Visual inspection	yellow solid	
Identity	MS (ESI)	521 [M+Na]	m/z
Identity	H-NMR	Con. to structure	ppm
Purity	H-NMR	< 5	Mass %
Optical Purity	H-NMR (de)	>98	% de
Purity	P-NMR	< 1	Mass %

Supplementary Figure 1. Quality assessment of HD5EU synthesis. a) Summary table listing all examined parameters and methodologies used to validate the structural conformity of the molecule and the purity of the product. **b)** MS Base Peak at 520.95 corresponding to $M+NA^+$ and at 1019 for $2M+NA^+$. **c)** ^{1}H-NMR conformity to structure. 513 MHz. DMSO as solvent. **d)** ^{31}p-NMR measurement for purity. 202.46 MHz. DMSO as solvent.

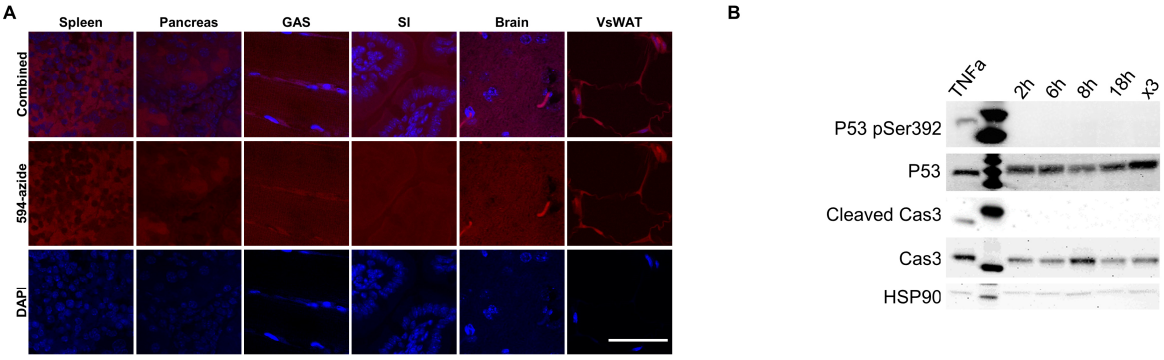

Supplementary Figure 2. Negative controls for in-vivo tissue staining. a) Click-it staining in tissues collected from saline treated animals. Scale Bar = 50µM. **b)** W.B. validating HD5EU safety. Lack of p53 activation and downstream Caspase cleavage at multiple time points following administrations of HD5EU and following consecutive administration of HD5EU. MEFs treated with TNFa for 16 hours serve as positive controls for the western blot staining.

651

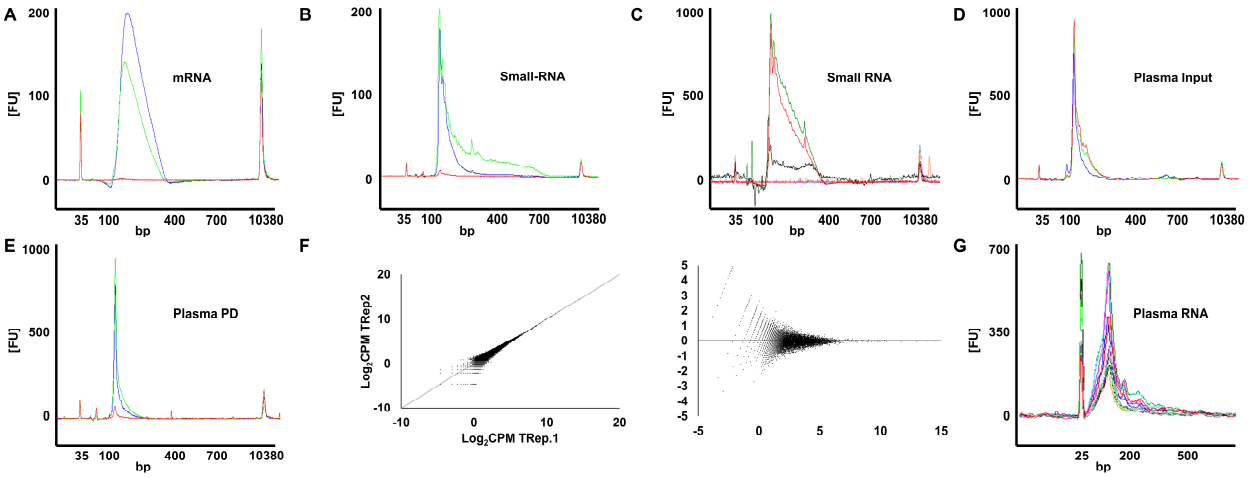

652

653 **Supplementary Figure 3. Specificity and reproducibility of RNA pull-down, library**
654 **construction and sequencing. A)** Bio-analyzer plot for mRNA Pull-down libraries. Blue -
655 HD5EU labelled liver, Green - HD5EU labelled kidney, Red - saline treated liver. We consistently
656 failed to generated libraries from non-labeled RNA subject to biotinylation and pull-down. **B)** Bio-
657 analyzer plot for small RNA pull-down libraries. Blue – HD5EU labelled liver, Green - HD5EU
658 labelled kidney, Red – Saline treated liver. **C)** Consistent failures in library generation from small
659 RNA (<200bp) pull-down in multiple tissue following 2h HD5EU treatment (Testis = orange,
660 VsWAT = pink and blue = Spleen). Input RNA generates expected library amplicons (Black, red
661 and green). **D)** Bio-analyzer plots for small RNA input libraries from plasma. **E)** Bio-analyzer
662 plots for small RNA pull-down libraries from plasma following multiple injections. Unlabeled
663 RNA in Red is amplified as input but fails to amplify following Pull-down. **F)** Scatter plot and
664 MA plot for two technical replicates from HD5EU labeled hepatocyte samples. Pearson correlation
665 coefficient = 0.95. **G)** Plasma ccfRNAs' size distribution.

666

667 **Supplementary Tables:**

668 **Supplementary table 1.** Identification and separation of various modified and unmodified
669 transcripts in LC-MS.

670 **Supplementary table 2.** Noiseq-bio analysis for the detection of enriched and depleted transcripts
671 following pull-down of labelled poly-A RNA in liver and kidney.

672 **Supplementary table 3.** GO and gene set enrichment analysis for kidney pulled-down and
673 depleted poly-A RNA.

674 **Supplementary table 4.** GO and gene set enrichment analysis for liver pulled-down and depleted
675 poly-A RNA.
676 **Supplementary table 5.** Differential expression analysis using Deseq2, for the detection of dietary
677 induced DEG in liver, input and pull-down poly-A RNA libraries.
678 **Supplementary table 6.** Differential expression analysis using Deseq2, for the detection of dietary
679 induced DEG in kidney, input and pull-down poly-A RNA libraries.
680 **Supplementary table 7.** GO and gene set enrichment analysis on dietary induced differentially
681 expressed genes in liver and kidney pull-down or depleted poly-A RNA.
682 **Supplementary table 8.** Noiseqbio differential pull-down analysis for liver, plasma and VsWAT
683 under HFD regime. TMM normalized mean expression values.
684 **Supplementary table 9.** Noiseqbio differential pull-down analysis for liver, plasma and VsWAT
685 under LFD regime. TMM normalized mean expression values.
686 **Supplementary table 10.** SuperExacttest package output. Overlaps between different sets and
687 calculated P.V.
688 **Supplementary table 11** GO and gene set enrichment analysis on plasma pulled-down protein
689 coding genes.
690 **Supplementary table 12** Differential expression analysis using Deseq2 package, for the detection
691 of dietary induced DEG in total VsWAT RNA.
692

693 **Reference:**

694 1. Murillo, O.D., et al., *exRNA Atlas Analysis Reveals Distinct Extracellular RNA Cargo Types and Their*
695 *Carriers Present across Human Biofluids.* Cell, 2019. **177**(2): p. 463-477 e15.
696 2. Yeri, A., et al., *Total Extracellular Small RNA Profiles from Plasma, Saliva, and Urine of Healthy*
697 *Subjects.* Sci Rep, 2017. **7**: p. 44061.
698 3. Dror, S., et al., *Melanoma miRNA trafficking controls tumour primary niche formation.* Nat Cell
699 Biol, 2016. **18**(9): p. 1006-17.
700 4. Castano, C., et al., *Obesity-associated exosomal miRNAs modulate glucose and lipid metabolism*
701 *in mice.* Proc Natl Acad Sci U S A, 2018. **115**(48): p. 12158-12163.
702 5. Wortzel, I., et al., *Exosome-Mediated Metastasis: Communication from a Distance.* Dev Cell, 2019.
703 **49**(3): p. 347-360.
704 6. Schwarzenbach, H., et al., *Clinical relevance of circulating cell-free microRNAs in cancer.* Nature
705 Reviews Clinical Oncology, 2014. **11**: p. 145.
706 7. Gilad, S., et al., *Serum microRNAs are promising novel biomarkers.* PLoS One, 2008. **3**(9): p. e3148.
707 8. Pegtel, D.M., et al., *Functional delivery of viral miRNAs via exosomes.* Proc Natl Acad Sci U S A,
708 2010. **107**(14): p. 6328-33.
709 9. Vickers, K.C., et al., *MicroRNAs are transported in plasma and delivered to recipient cells by high-*
710 *density lipoproteins.* Nat Cell Biol, 2011. **13**(4): p. 423-33.

711 10. Pastuzyn, E.D., et al., *The Neuronal Gene Arc Encodes a Repurposed Retrotransposon Gag Protein*
712 *that Mediates Intercellular RNA Transfer.* Cell, 2018. **172**(1-2): p. 275-288 e18.
713 11. Kosaka, N., et al., *Secretory mechanisms and intercellular transfer of microRNAs in living cells.* J
714 Biol Chem, 2010. **285**(23): p. 17442-52.
715 12. Thomou, T., et al., *Adipose-derived circulating miRNAs regulate gene expression in other tissues.*
716 Nature, 2017. **542**(7642): p. 450-455.
717 13. Sharma, U., et al., *Small RNAs Are Trafficked from the Epididymis to Developing Mammalian*
718 *Sperm.* Dev Cell, 2018. **46**(4): p. 481-494 e6.
719 14. Gay, L., et al., *Mouse TU tagging: a chemical/genetic intersectional method for purifying cell type-*
720 *specific nascent RNA.* Genes Dev, 2013. **27**(1): p. 98-115.
721 15. Herzog, V.A., et al., *Thiol-linked alkylation of RNA to assess expression dynamics.* Nat Methods,
722 2017. **14**(12): p. 1198-1204.
723 16. Chatzi, C., et al., *Transcriptional Profiling of Newly Generated Dentate Granule Cells Using TU*
724 *Tagging Reveals Pattern Shifts in Gene Expression during Circuit Integration.* eNeuro, 2016. **3**(1).
725 17. Miller, M.R., et al., *TU-tagging: cell type-specific RNA isolation from intact complex tissues.* Nat
726 Methods, 2009. **6**(6): p. 439-41.
727 18. Ghosh, A.C., et al., *UPRT, a suicide-gene therapy candidate in higher eukaryotes, is required for*
728 *Drosophila larval growth and normal adult lifespan.* Sci Rep, 2015. **5**: p. 13176.
729 19. Maquat, L.E. and M. Kiledjian, *RNA turnover in eukaryotes: nucleases, pathways and analysis of*
730 *mRNA decay. Preface.* Methods Enzymol, 2008. **448**: p. xxi-xxii.
731 20. Hida, N., et al., *EC-tagging allows cell type-specific RNA analysis.* Nucleic Acids Res, 2017. **45**(15):
732 p. e138.
733 21. Song, A.J. and R.D. Palmiter, *Detecting and Avoiding Problems When Using the Cre-lox System.*
734 Trends Genet, 2018. **34**(5): p. 333-340.
735 22. Alberti, C., et al., *Cell-type specific sequencing of microRNAs from complex animal tissues.* Nat
736 Methods, 2018. **15**(4): p. 283-289.
737 23. Marquart, T.J., et al., *miR-33 links SREBP-2 induction to repression of sterol transporters.* Proc Natl
738 Acad Sci U S A, 2010. **107**(27): p. 12228-32.
739 24. Rayner, K.J., et al., *MiR-33 contributes to the regulation of cholesterol homeostasis.* Science, 2010.
740 **328**(5985): p. 1570-3.
741 25. Zheng, L., et al., *Effect of miRNA-10b in regulating cellular steatosis level by targeting PPAR-alpha*
742 *expression, a novel mechanism for the pathogenesis of NAFLD.* J Gastroenterol Hepatol, 2010.
743 **25**(1): p. 156-63.
744 26. Lee, E.K., et al., *miR-130 suppresses adipogenesis by inhibiting peroxisome proliferator-activated*
745 *receptor gamma expression.* Mol Cell Biol, 2011. **31**(4): p. 626-38.
746 27. Jao, C.Y. and A. Salic, *Exploring RNA transcription and turnover in vivo by using click chemistry.*
747 Proc Natl Acad Sci U S A, 2008. **105**(41): p. 15779-84.
748 28. Best, M.D., *Click chemistry and bioorthogonal reactions: unprecedented selectivity in the labeling*
749 *of biological molecules.* Biochemistry, 2009. **48**(28): p. 6571-84.
750 29. Hagemeijer, M.C., et al., *Visualizing coronavirus RNA synthesis in time by using click chemistry.* J
751 Virol, 2012. **86**(10): p. 5808-16.
752 30. Gierlich, J., et al., *Click chemistry as a reliable method for the high-density postsynthetic*
753 *functionalization of alkyne-modified DNA.* Org Lett, 2006. **8**(17): p. 3639-42.
754 31. Meyer, J.P., et al., *Click Chemistry and Radiochemistry: The First 10 Years.* Bioconjug Chem, 2016.
755 **27**(12): p. 2791-2807.
756 32. Pradere, U., et al., *Synthesis of nucleoside phosphate and phosphonate prodrugs.* Chem Rev, 2014.
757 **114**(18): p. 9154-218.

758 33. Erion, M.D., et al., *Design, synthesis, and characterization of a series of cytochrome P(450) 3A-*
759 *activated prodrugs (HepDirect prodrugs) useful for targeting phosph(on)ate-based drugs to the*
760 *liver.* J Am Chem Soc, 2004. **126**(16): p. 5154-63.
761 34. Boyer, S.H., et al., *Synthesis and characterization of a novel liver-targeted prodrug of cytosine-1-*
762 *beta-D-arabinofuranoside monophosphate for the treatment of hepatocellular carcinoma.* J Med
763 Chem, 2006. **49**(26): p. 7711-20.
764 35. Erion, M.D., et al., *Targeting thyroid hormone receptor-beta agonists to the liver reduces*
765 *cholesterol and triglycerides and improves the therapeutic index.* Proc Natl Acad Sci U S A, 2007.
766 **104**(39): p. 15490-5.
767 36. Reddy, K.R., et al., *Pradefovir: a prodrug that targets adefovir to the liver for the treatment of*
768 *hepatitis B.* J Med Chem, 2008. **51**(3): p. 666-76.
769 37. van Herwaarden, A.E., et al., *Midazolam and cyclosporin a metabolism in transgenic mice with*
770 *liver-specific expression of human CYP3A4.* Drug Metab Dispos, 2005. **33**(7): p. 892-5.
771 38. van Herwaarden, A.E., et al., *Knockout of cytochrome P450 3A yields new mouse models for*
772 *understanding xenobiotic metabolism.* J Clin Invest, 2007. **117**(11): p. 3583-92.
773 39. Simonet, W.S., et al., *A far-downstream hepatocyte-specific control region directs expression of*
774 *the linked human apolipoprotein E and C-I genes in transgenic mice.* J Biol Chem, 1993. **268**(11):
775 p. 8221-9.
776 40. Stresser, D.M., et al., *Highly selective inhibition of human CYP3Aa in vitro by azamulin and*
777 *evidence that inhibition is irreversible.* Drug Metab Dispos, 2004. **32**(1): p. 105-12.
778 41. Su, D., et al., *Quantitative analysis of ribonucleoside modifications in tRNA by HPLC-coupled mass*
779 *spectrometry.* Nat Protoc, 2014. **9**(4): p. 828-41.
780 42. Williams, L.M., et al., *The development of diet-induced obesity and glucose intolerance in C57BL/6*
781 *mice on a high-fat diet consists of distinct phases.* PLoS One, 2014. **9**(8): p. e106159.
782 43. Dobin, A., et al., *STAR: ultrafast universal RNA-seq aligner.* Bioinformatics, 2013. **29**(1): p. 15-21.
783 44. Tarazona, S., et al., *Data quality aware analysis of differential expression in RNA-seq with NOISeq*
784 *R/Bioc package.* Nucleic Acids Res, 2015. **43**(21): p. e140.
785 45. Chen, E.Y., et al., *Enrichr: interactive and collaborative HTML5 gene list enrichment analysis tool.*
786 BMC Bioinformatics, 2013. **14**: p. 128.
787 46. Coudrier, E., D. Kerjaschki, and D. Louvard, *Cytoskeleton organization and submembranous*
788 *interactions in intestinal and renal brush borders.* Kidney Int, 1988. **34**(3): p. 309-20.
789 47. Lin, G., E. Finger, and J.C. Gutierrez-Ramos, *Expression of CD34 in endothelial cells, hematopoietic*
790 *progenitors and nervous cells in fetal and adult mouse tissues.* Eur J Immunol, 1995. **25**(6): p. 1508-
791 16.
792 48. Fina, L., et al., *Expression of the CD34 gene in vascular endothelial cells.* Blood, 1990. **75**(12): p.
793 2417-26.
794 49. Liu, Y., D.K. Qiu, and X. Ma, *Liver X receptors bridge hepatic lipid metabolism and inflammation.* J
795 Dig Dis, 2012. **13**(2): p. 69-74.
796 50. Kersten, S., et al., *Peroxisome proliferator-activated receptor alpha mediates the adaptive*
797 *response to fasting.* J Clin Invest, 1999. **103**(11): p. 1489-98.
798 51. Tyagi, S., et al., *The peroxisome proliferator-activated receptor: A family of nuclear receptors role*
799 *in various diseases.* J Adv Pharm Technol Res, 2011. **2**(4): p. 236-40.
800 52. Everett, L., A. Galli, and D. Crabb, *The role of hepatic peroxisome proliferator-activated receptors*
801 *(PPARs) in health and disease.* Liver, 2000. **20**(3): p. 191-199.
802 53. Park, J., et al., *Single-cell transcriptomics of the mouse kidney reveals potential cellular targets of*
803 *kidney disease.* Science, 2018. **360**(6390): p. 758-763.
804 54. MacParland, S.A., et al., *Single cell RNA sequencing of human liver reveals distinct intrahepatic*
805 *macrophage populations.* Nat Commun, 2018. **9**(1): p. 4383.

806 55. Love, M.I., W. Huber, and S. Anders, *Moderated estimation of fold change and dispersion for RNA-*
807 *seq data with DESeq2.* Genome Biol, 2014. **15**(12): p. 550.
808 56. Srinivasan, S., et al., *Small RNA Sequencing across Diverse Biofluids Identifies Optimal Methods for*
809 *exRNA Isolation.* Cell, 2019. **177**(2): p. 446-462 e16.
810 57. Wang, M., Y. Zhao, and B. Zhang, *Efficient Test and Visualization of Multi-Set Intersections.* Sci
811 Rep, 2015. **5**: p. 16923.
812 58. Liu, H., et al., *Escherichia coli noncoding RNAs can affect gene expression and physiology of*
813 *Caenorhabditis elegans.* Nat Commun, 2012. **3**: p. 1073.
814 59. Weiberg, A., et al., *Fungal small RNAs suppress plant immunity by hijacking host RNA interference*
815 *pathways.* Science, 2013. **342**(6154): p. 118-23.
816 60. Timmons, L. and A. Fire, *Specific interference by ingested dsRNA.* Nature, 1998. **395**(6705): p. 854.
817 61. Rivkin, M., et al., *Inflammation-Induced Expression and Secretion of MicroRNA 122 Leads to*
818 *Reduced Blood Levels of Kidney-Derived Erythropoietin and Anemia.* Gastroenterology, 2016.
819 **151**(5): p. 999-1010 e3.
820 62. Chai, C., et al., *Metabolic Circuit Involving Free Fatty Acids, microRNA 122, and Triglyceride*
821 *Synthesis in Liver and Muscle Tissues.* Gastroenterology, 2017. **153**(5): p. 1404-1415.
822 63. Rechavi, O., et al., *Cell contact-dependent acquisition of cellular and viral nonautonomously*
823 *encoded small RNAs.* Genes Dev, 2009. **23**(16): p. 1971-9.
824 64. Lee, Y.S., et al., *Inflammation is necessary for long-term but not short-term high-fat diet-induced*
825 *insulin resistance.* Diabetes, 2011. **60**(10): p. 2474-83.
826 65. Hotamisligil, G.S., *Inflammation and metabolic disorders.* Nature, 2006. **444**(7121): p. 860-7.
827 66. Chou, C.H., et al., *miRTarBase update 2018: a resource for experimentally validated microRNA-*
828 *target interactions.* Nucleic Acids Res, 2018. **46**(D1): p. D296-D302.
829 67. Portius, D., C. Sobolewski, and M. Foti, *MicroRNAs-Dependent Regulation of PPARs in Metabolic*
830 *Diseases and Cancers.* PPAR Res, 2017. **2017**: p. 7058424.
831 68. Horie, T., et al., *MicroRNA-33 regulates sterol regulatory element-binding protein 1 expression in*
832 *mice.* Nat Commun, 2013. **4**: p. 2883.
833 69. Shimano, H., *SREBPs: physiology and pathophysiology of the SREBP family.* FEBS J, 2009. **276**(3):
834 p. 616-21.
835 70. Kirchner, S. and Z. Ignatova, *Emerging roles of tRNA in adaptive translation, signalling dynamics*
836 *and disease.* Nat Rev Genet, 2015. **16**(2): p. 98-112.
837 71. Enache, L.S., et al., *Circulating RNA molecules as biomarkers in liver disease.* Int J Mol Sci, 2014.
838 **15**(10): p. 17644-66.
839 72. Thul, P.J., et al., *A subcellular map of the human proteome.* Science, 2017. **356**(6340).
840 73. Balcells, I., S. Cirera, and P.K. Busk, *Specific and sensitive quantitative RT-PCR of miRNAs with DNA*
841 *primers.* BMC Biotechnol, 2011. **11**: p. 70.
842 74. Busk, P.K., *A tool for design of primers for microRNA-specific quantitative RT-qPCR.* BMC
843 Bioinformatics, 2014. **15**: p. 29.
844 75. Chan, P.P. and T.M. Lowe, *GtRNAdb 2.0: an expanded database of transfer RNA genes identified*
845 *in complete and draft genomes.* Nucleic Acids Res, 2016. **44**(D1): p. D184-9.

846